CRYSTAL GROWTH & DESIGN

pubs.acs.org/crystal

Article

Mechanically Induced Amorphization of Diaqua-bis(Omeprazolate)-Magnesium Dihydrate

Hanane Abouhakim, Michael J. Quayle,* Stefan T. Norberg, Sten O. Nilsson Lill, Maryam Asachi, Sven L. M. Schroeder, Frans L. Muller, and Ali Hassanpour*

Cite This: *Cryst. Growth Des.* 2020, 20, 6057−6068

Read Online

ACCESS | Metrics & More | Article Recommendations | Supporting Information

ABSTRACT: The influence of milling diaqua-bis(omeprazolate)-magnesium dihydrate (DABOMD), an active pharmaceutical ingredient (API), was investigated. DABOMD was processed in a planetary ball mill at different milling times, from 1 to 300 min. The milling process resulted in a prominent comminution (size reduction) and amorphization of the API. DABOMD amorphization was identified with various characterization techniques including thermogravimetric analysis, differential scanning calorimetry, powder X-ray diffraction, and attenuated total reflection-Fourier transform infrared spectroscopy. The solid−solid crystalline to amorphous phase transformation is driven by compression, shear stresses, and heat generated in the planetary ball mill. This leads to distortion and breakage of hydrogen bonds, release of water molecules from the crystalline lattice of DABOMD and the accumulation of defects, and eventually a collapse of the crystalline order. Model fitting of the kinetics of comminution and the amorphization of DABOMD revealed a series of events: a rapid comminution at the start of milling driven by crystal cleavage of DABOMD, followed by partial amorphization, which is driven by rapid water diffusion, and subsequently, a slow steady comminution and amorphization.

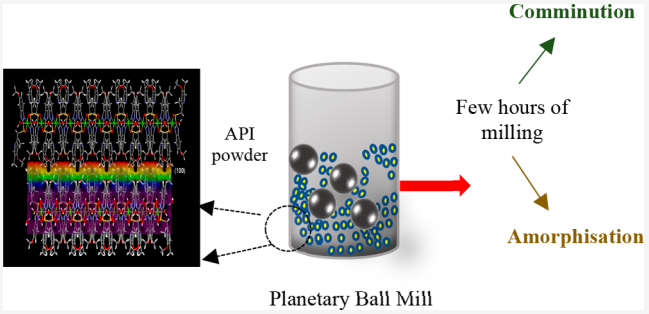

1. INTRODUCTION

Milling is a very important operation for the comminution (size reduction) and homogeneity of particles. It is often used in the pharmaceutical industry to optimize the dissolution rate of poorly soluble drugs, enhance the bioavailability, facilitate tablet compression, and permit a more accurate dosing of the drugs.[1−3] Nonetheless, excessive energy from the mill can lead to crystalline lattice disruption and solid form transformations, including amorphization.[3−5] The physicochemical changes that arise from the excessive energy during milling are referred to as mechanochemistry, whereas the milling/grinding processes that cause these changes are referred to as mechanical activation.[6−10] The impact of mechanical activation remains unpredictable in many ways. It is widely accepted that amorphization through a milling process can improve the solubility of drugs. No controlled studies have been conducted to cover all the aspects of this transformation during milling. Hence, special consideration of the possible amorphization of the drug during milling is needed,[11,12] including conducting a controlled experiment and understanding the mechanisms of which such transformations occur.

During milling, particles are reduced by impact, shear, attrition, and compression or a combination of these stress modes.[13] The stresses arising might contribute to different influences on the product. The mechanical activation of solid pharmaceuticals is attributed to the change in their physical and chemical properties including reactivity, solubility, and bioavailability.[14] The change induced in solid pharmaceutical reactivity is associated with the formation of defects, distortion, and disordering of the crystal structure and eventually the disappearance of the order of the atoms and molecules present in the crystal, i.e., the formation of amorphous material. For instance, milling of Cephalexin results in the formation of amorphous material, which attributes to enhancing its dissolution rates.[15] Similarly, milling of Griseofulvin leads to the formation of amorphous material on its surface layers, which also enhances its dissolution rate. Piroxicam is not soluble in water, which implies it has lower bioavailability. Mechanical treatment of the drug causes a change in the crystal structure of Piroxicam as well as in its reactivity, which increases the drug solubility four times compared to the nonmilled compound.[16]

In addition to the formation of amorphous material, mechanical activation can promote the transition from one

Received: June 5, 2020
Revised: July 23, 2020
Published: July 28, 2020

https://dx.doi.org/10.1021/acs.cgd.0c00770
Cryst. Growth Des. 2020, 20, 6057−6068

crystalline form to another. For instance, the polymorphic transition from a metastable form of Carbamazepine to the stable β-form leads to a reduction in compressibility and enhanced stability. The extent of change caused to the drug as a result of milling the API depends on the condition under which milling is performed as well as the API material properties.

To investigate the impact of mechanical treatment on a crystalline solid pharmaceutical, one should consider the glass-forming ability (formation of amorphous) and the physical stability since this will allow screening for the most stable compound to avoid any potential recrystallization before the process of analysis. Mahlin et al. 2013 developed a model to predict the glass-forming ability and physical stability and found that samples that possess a large molecular weight (M_w > 300 g/mol) and a high glass transition temperature can form an amorphous form with long lasting stability (≥1 month).[17] On the basis of this model and on other aspects including safety and costs, a candidate API was chosen for the mechanical treatment study. Diaqua-bis(omeprazolate)-magnesium dihydrate (DABOMD) (Figure 1), which is the salt form of omeprazole and sold under the brand Losec, was selected for this work. Omeprazole (IUPAC name 6-methoxy-2-[(4-methoxy-3,5-dimethyl-2-pyridyl)methylsulfonyl]-1*H*-benzimidazole) is a pharmaceutical drug developed for the treatment of stomach acid reflux and gastrointestinal inflammatory-related diseases.[18,19] In this work, a planetary ball mill (Figure 2) was employed for mechanical activation since it has been commonly reported for inducing amorphization as a result of the high energy involved in the process of size reduction. Examples of pharmaceuticals reported to change from crystalline to amorphous phase upon planetary ball milling include Linaprazan,[20] Budesonide,[21] Sulfathiazole,[22,23] Indomethacin,[15] and Fananserine.[24]

2. MATERIALS AND METHODS

2.1. Materials. In this work, two solid-state forms of DABOMD were used, a crystalline and an amorphous powder. The crystalline powder of racemic DABOMD (*R*- and *S*-form) with 98% purity was provided by AstraZeneca.

Amorphous powder of DABOMD was prepared from a DABOMD/methanol solution (approximately 18 g in 0.7 L) followed by a rapid evaporation in a rotary evaporator at 40 °C and 20 mbar. Subsequently, the product was further dried in a vacuum (10 mbar). The amorphous form was confirmed by the absence of Braggs peaks in powder X-ray diffraction (PXRD).

2.2. Methods. *2.2.1. Milling Experiment.* DABOMD crystalline powder was milled using a Retsch PM100 planetary ball mill (PBM). The powder samples were milled between 1 and 300 min at a speed of 650 rpm in 250 mL steel jar using four 15 mm diameter at a ball to powder ratio (BPR) of 10:1 by weight. The BPR allows for increased contacts and better particle breakage and size reduction.[25]

2.2.2. Powder Characterization. The nonmilled and the milled samples were characterized to determine their morphological, size, crystalline, and thermodynamic properties, in addition to the intermolecular characteristics from the crystal structure.

Morphology. Surface and morphological properties of DABOMD were examined using scanning electron microscope (SEM) in a Carl Zeiss EVO MA15 scanning electron microscope at 20 kV in backscattered imaging mode. Carbon tabs were coated with powder samples and placed on SEM metal stubs. Sample stubs were sputter-coated with a conductive layer of platinum before the analysis to prevent charging.

Particles Size Analysis. The particle size distribution (PSD) was analyzed by the laser diffraction method (in a Malvern 3000) of dry sample powders. The powder was dispersed in air at a pressure of 2 bar, a feed rate of 50%, and with obscuration ranging from 2 to 10%.

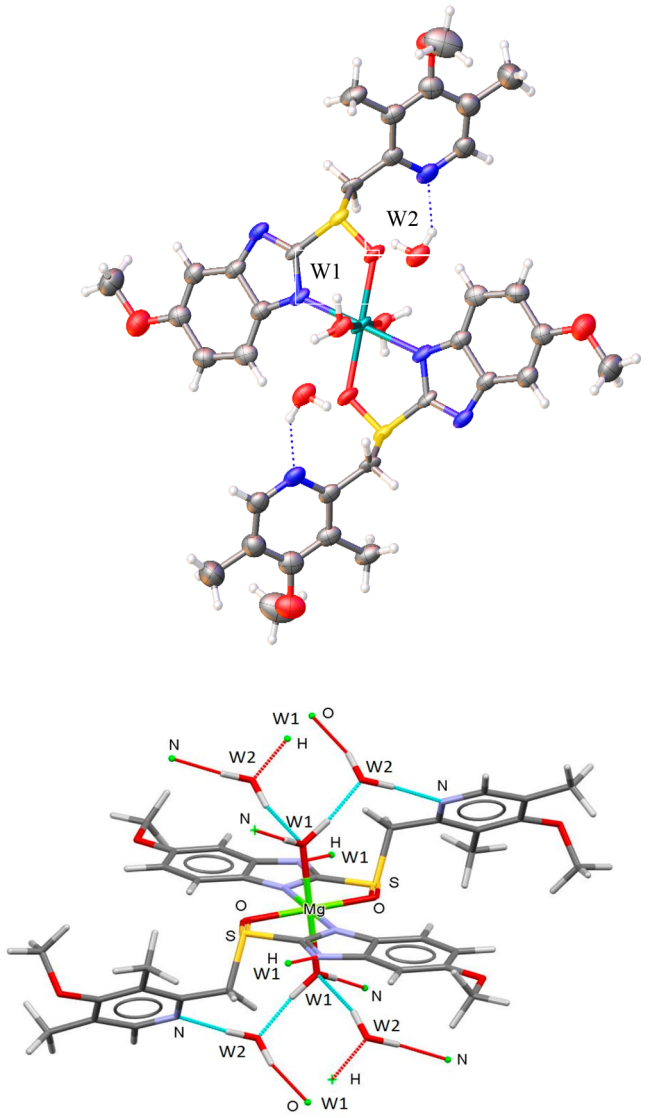

Figure 1. (Top) Molecular structure of diaqua-bis (Omeprazolate)-magnesium dihydrate (DABOMD). Intermolecular hydrogen bonding between the molecules in the lattice shown in blue dotted lines Mg: green, S: yellow, N: blue, O: red, C: gray, H: white. Reproduced with the permission of the International Union of Crystallography (IUCr).[31] (Bottom) Hydrogen bond network in diaqua-bis (Omeprazolate)-magnesium dihydrate (DABOMD). Mg: green, S: yellow, N: blue, O: red, C: gray, H: white.

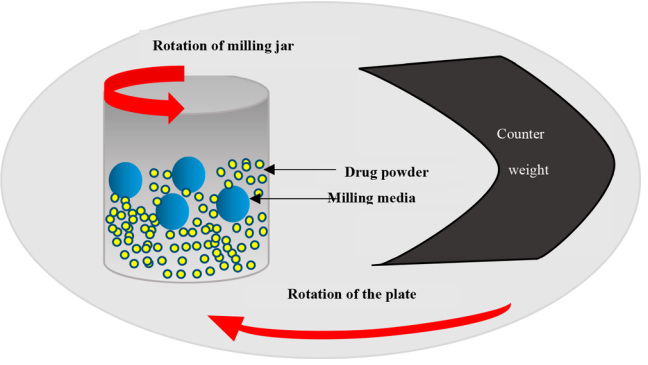

Figure 2. Schematic diagram of a planetary ball mill.

https://dx.doi.org/10.1021/acs.cgd.0c00770
Cryst. Growth Des. 2020, 20, 6057−6068

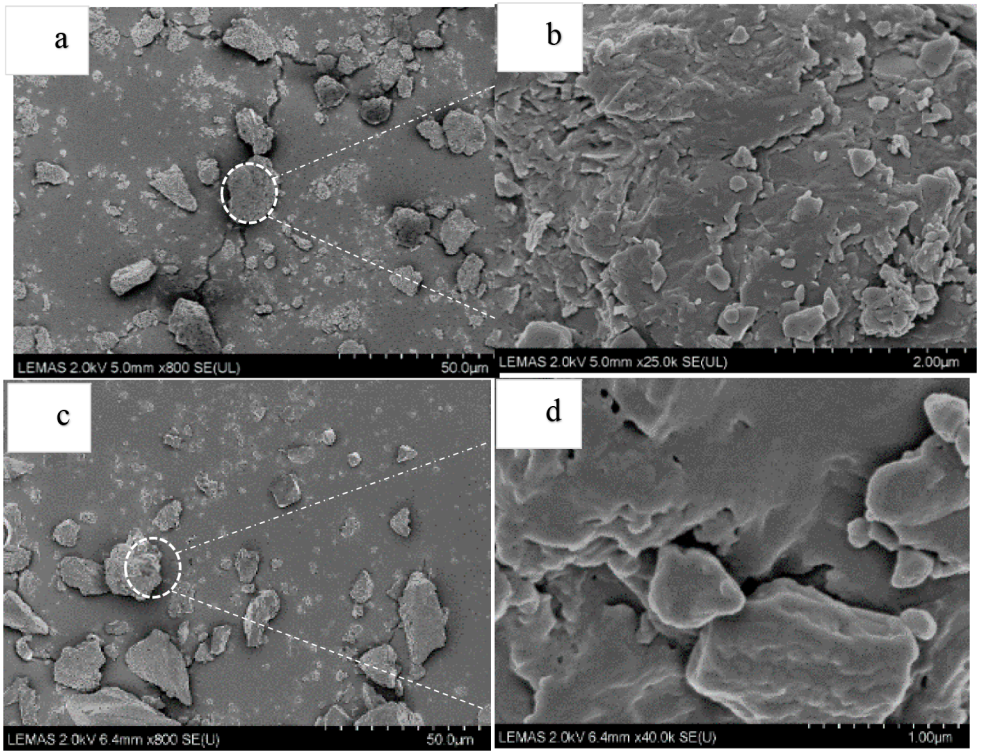

Figure 3. SEM images show the morphology of DABOMD, (a) nonmilled (×800), (b) nonmilled (×25000), (c) 300 min milled (×800), (d) 300 min milled (×25000).

Thermodynamic Properties. Differential scanning calorimetry (DSC) analysis of the nonmilled and milled DABOMD was carried out using a Mettler TC 3000 differential scanner calorimeter with purged liquid nitrogen at a rate 5 °C/min from 25 to 250 °C. Approximately 5−6 mg of powder was placed in an aluminum sealed pan with a small hole in the top. Similarly, thermogravimetric analysis (TGA) was carried out with a flowing gaseous nitrogen and a rate 5 °C/min from 25 to 250 °C. TA Instruments Universal analysis 2000 was used for the analysis step.

Crystalline Properties. The crystalline properties of the milled powder were analyzed using powder X-ray diffraction (PXRD) with a Phillips PW 1710 X-ray diffractometer using a Cu Kα radiation (λ = 0.14406 nm) operating with 40 kV accelerated voltage and 30 mA current. Scans were collected over a 2θ range from 5° to 55°, scanned in steps of 0.02°, with a dwell time of 0.25 s and 3° slit in front of the detector.

Intermolecular Properties. Attenuated total reflectance-Fourier transform infrared (ATR-FTIR) spectroscopy measurements were carried out on an ATR-FTIR thermo iS101 to analyze the effect of milling on the intermolecular properties of the sample. FTIR analysis of the nonmilled powder, milled samples, and amorphous standard powder was carried out at a range from 400 to 4000 cm^{-1}. A background spectrum was obtained for each experimental condition, and 37 scans were taken for each sample. Computed IR spectra was generated for a geometry optimized representative molecular model system (see Figure S3 in the Supporting Information) using B3LYP-D3/6-31G(d,p) as implemented in Jaguar 10.7.[26] A few atomic positions were fixed in the optimization in order to keep the feature of the influence of the periodic crystal structure. This is a standard procedure for modeling for example enzymatic reactions.[27] These positions are marked in Figure S3.

Quantification of Solid Phases. The mole fraction x_j of crystalline and amorphous DABOMD in samples taken before and after milling was quantified using a chemometric linear combination of FTIR spectra. All the quantifications were conducted in the MATLAB R201 software using a code that was previously established for the measurement of different components in detergent powder mixtures using near infrared (NIR).[28] A spectrum consists of N_k intensities (I) measured at a specific wavenumber (λ_k). Spectrum pretreatment was carried out using first and second (dI', dI'') derivatives to remove the offset and baseline shifts arising from differing particle sizes[28,29] as shown in eqs 1 and 2.

$$dI'(\lambda_k) = \frac{I(\lambda_{k+1}) - I(\lambda_k)}{\lambda_{k+1} - \lambda_k} \quad (1)$$

$$dI''(\lambda_k) = \frac{I(\lambda_{k+1}) - I(\lambda_k) + I(\lambda_{k-1})}{(\lambda_{k+1} - \lambda_k)^2} \quad (2)$$

Calculation of the solid phases using FTIR spectra was conducted according to the Johanson (2014)[30] approach shown in eq 3. This assumes the surface consists of either crystalline or amorphous domains, and the intensity of reflected light is determined by the surface area fraction of those two respective domains:

$$dI_{mix.pred}(\lambda, f_{AAC}) = f_{AAC}\, dI_{amp}(\lambda) + (1 - f_{AAC})\, dI_{cryst}(\lambda) \quad (3)$$

Here, f_{AAC} is the area fraction of amorphous material on the surface of the particles. The predicted first- or second-order derivative spectrum $dI_{mix.pred}$ (eqs 1 or 2) contains surface averaged contributions of the derivatives of the amorphous and crystalline reference spectra dI_{amp} and dI_{cryst}.

For a specific samples' spectrum, the amorphous content f_{AAC} is obtained by minimization of the sum of residual differences squared (SOS) between the experimental FTIR intensity of mixture $dI_{mix}(\lambda)$ and calculated value as displayed in eq 4.

$$\min_{f_{AAC}} SOS = \min_{f_{AAC}} \left[\sum_{k=1}^{N_k} (dI_{mix}(\lambda_k) - dI_{mix.pred}(\lambda_k, F_{AAC}))^2 \right] \quad (4)$$

3. RESULTS AND DISCUSSION

3.1. Powder Characterization. *3.1.1. Morphology of Particles.* Representative SEM images of the nonmilled and

https://dx.doi.org/10.1021/acs.cgd.0c00770
Cryst. Growth Des. 2020, 20, 6057−6068

milled powders of DABOMD from 1 to 300 min are shown in Figure 3 (Figures S1 and S2 in the Supporting Information). It can be observed that the nonmilled particles have irregular shapes with varying size distribution and some agglomerated crystals (which are low in number but high in volume). As the milling proceeds, the deagglomeration process takes place, but some of the produced fine particles can be observed to adhere to the surface of larger ones; see for example in Figure 3d.

3.1.2. Particle Size Distribution. The PSD, the cumulative distribution, and the characteristic sizes of the nonmilled and the milled powders of DABOMD are shown in Figures 4 and 5 as

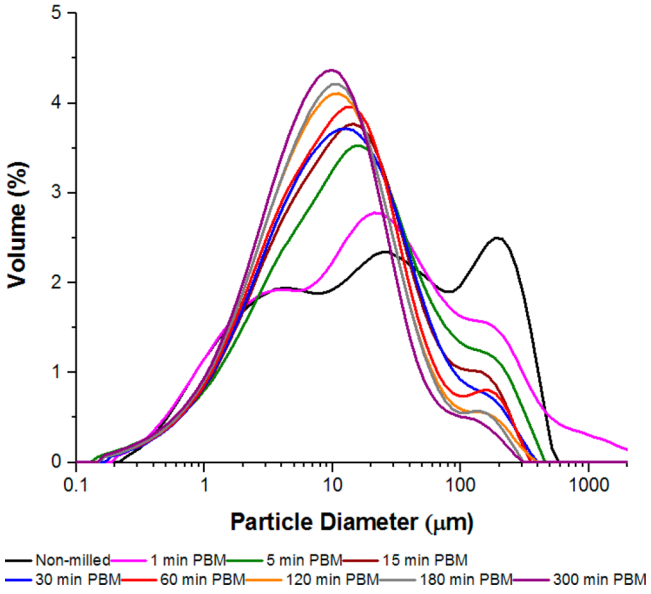

Figure 4. Particle size distribution of nonmilled and planetary ball milled DABOMD from 1 to 300 min.

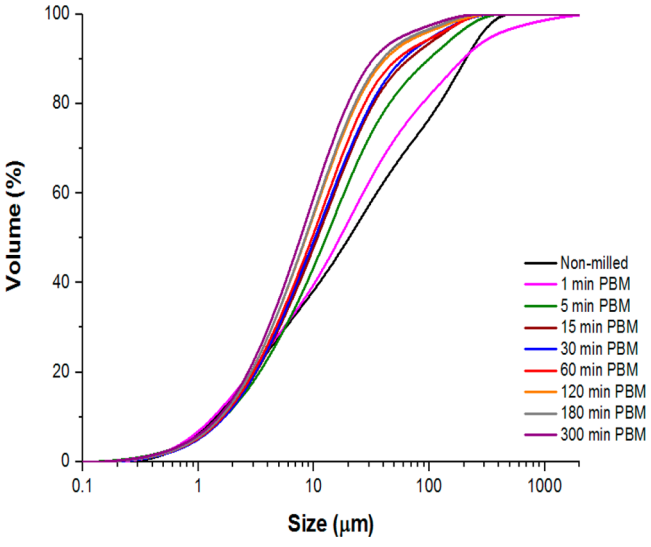

Figure 5. Cumulative particle size distribution of nonmilled and planetary ball milled DABOMD from 1 to 300 min.

well as in Table 1. The milling process caused a significant reduction in D_{50} (median diameter) and D_{90} (diameter representing 90% of the distribution) over time. The as-received nonmilled material has a trimodal profile due to the presence of particles with various sizes and some agglomerates which

Table 1. Characteristic Sizes (D_{10}, D_{50}, and, D_{90}) of Nonmilled and Milled DABOMD Samples in Planetary Ball Mill from 1 to 300 min

	particle size (μm)		
sample	D_{10}	D_{50}	D_{90}
nonmilled	1.5	21.2	211.0
1 min	1.5	16.4	180.0
5 min	1.7	12.7	98.1
15 min	1.7	11.2	66.9
30 min	1.7	9.9	58.9
60 min	1.7	9.9	51.8
120 min	1.6	8.7	45.6
180 min	1.7	8.7	40.1
300 min	1.5	7.5	35.3

transformed into a narrower profile centered around 10 μm as the milling progressed. There was a significant size reduction between the as-received nonmilled samples and the samples milled for 300 min. The nonmilled sample had a D_{90} of 211 μm and, the 300 min milled sample had a D_{90} of 35 μm. Interestingly, the cumulative size distribution depicted in Figure 4 shows a significant size reduction between the nonmilled and the 15 min milled samples due to the deagglomeration process, followed by a steady size reduction between 15 and 300 min of milling. Moreover, the PSD analysis shows that milling for 1 min promotes some agglomeration that occurs as a result of the formation and adhesion of fines to the larger particles. Analysis of the fines concentration as a function of time showed negligible variation in D_{10} (diameter representing 10% of the distribution), which is likely to be within the resolution limit of the laser diffraction measurement method.

3.1.3. Crystalline Properties. PXRD of crystalline nonmilled DABOMD exhibits a series of sharp peaks corresponding to the crystalline material, whereas that of standard amorphous material possesses a typical halo peak with two broad maxima at $2\theta = 17.5°$ and 24° respectively as shown in Figure 6. As the milling progresses, the PXRD patterns change rapidly with both a reduction in intensity as well as broadening of the Bragg peaks

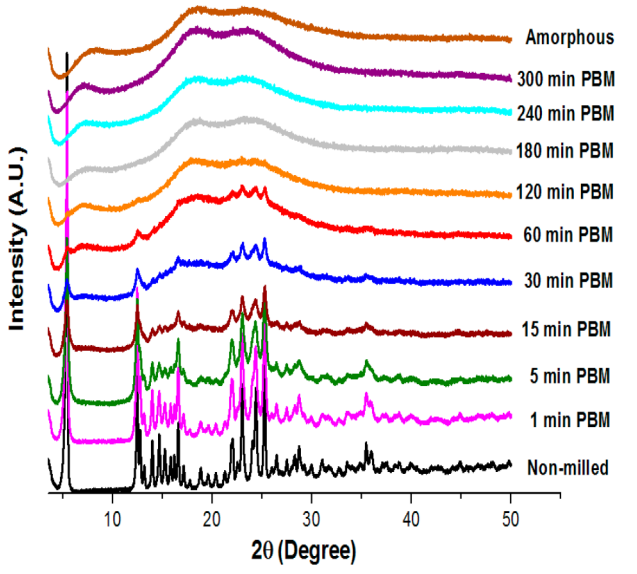

Figure 6. PXRD of DABOMD before milling and after milling with a planetary ball mill from 1 to 300 min.

https://dx.doi.org/10.1021/acs.cgd.0c00770
Cryst. Growth Des. 2020, 20, 6057−6068

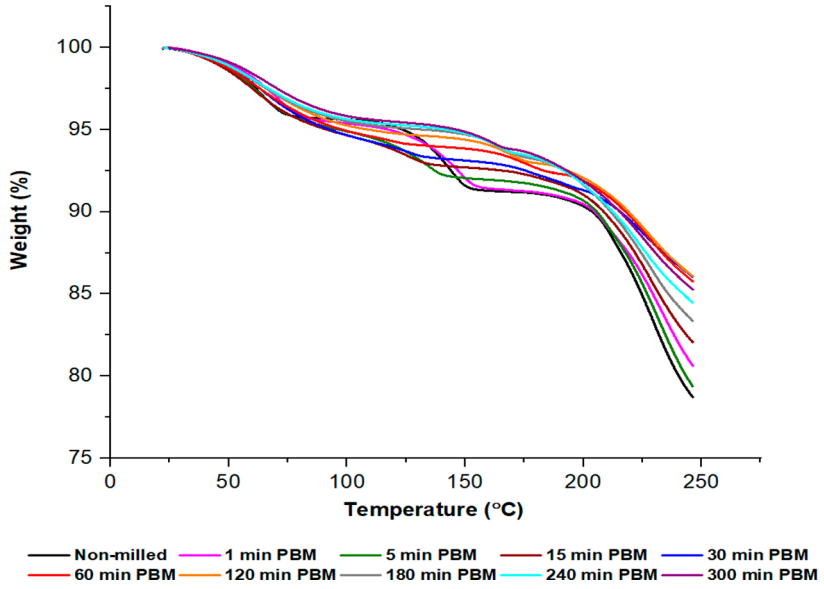

Figure 7. TGA profile of DABOMD for the nonmilled and milled with a planetary ball mill at a temperature of 25−250 °C and a rate 5 °C/min.

evident, which indicates a solid transition from crystalline to amorphous. Beyond 60 min sharp Braggs peaks, characteristics for a crystalline are absent, a typical scattering pattern for materials without long-range order observed.

3.1.4. Thermodynamic Properties. DSC and TGA analyses were performed to evaluate the effect of milling on the thermochemical properties of DABOMD. For the crystalline nonmilled sample, the TGA profile shown in Figure 7 has two mass losses corresponding to two types of water interactions present in the crystalline lattice. This was described in a previous study.[31] As the milling progresses, it appears that the amount of mass loss detected by TGA reduces significantly with milling time, which suggests that milling promotes dehydration, reflected in the release of water molecules from the crystalline lattice. This outcome agrees with the change in the crystalline properties detected by PXRD. The TGA pattern obtained for the milled samples (120 min and longer) of DABOMD is analogous to that reported for amorphous Esomeprazole magnesium[32] prepared by vacuum drying. Similarly, it has previously been suggested that sodium Omeprazole undergoes amorphization as a result of drying.[33]

The DSC analysis of crystalline nonmilled DABOMD shows three distinct thermal events: two endothermic and one exothermic at 109 °C, 173 °C, and, 197.8 °C, respectively (Figure 8). The first endothermic peaks represent a water loss event, while the second endothermic peak corresponds to the loss of more strongly bonded water. The third exothermic peak represents the decomposition of DABOMD.[31]

As the milling progresses, the DSC profile for the milled sample (Figure 8) shows that the peak intensity continuously reduces with milling time and shifts to lower temperatures consistent with a loss of crystallinity. The thermal behavior of the longer milled sample is analogous to that of amorphous Esomeprazole magnesium.[32] Overall, thermochemical analyses suggest that the phase transformation of DABOMD is driven by the sequential dehydration processes during milling.

3.1.5. Intermolecular Interactions. The phase transformation from crystalline to amorphous occurs as a result of a change in the molecular interactions. These interactions can be in the form of hydrogen bonds, which play an important role in the

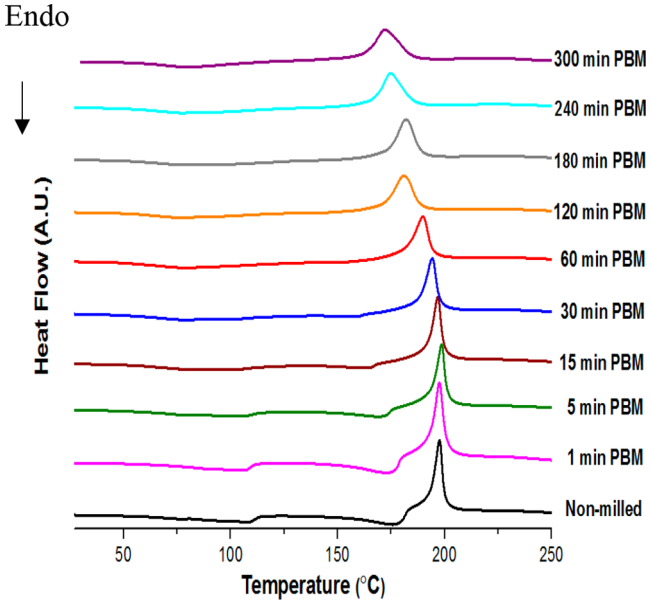

Figure 8. DSC profile of DABOMD for the nonmilled and milled with a planetary ball mill at a temperature of 25−250 °C and a rate 5 °C/min.

crystalline packing, in addition to weaker interactions such as van der Waals interactions, or electrostatic interactions.[34] Fourier transform infrared (FTIR) spectroscopy is sensitive to the level of order and disorder present in the crystal structure, including changes in hydrogen bonding[35,36] and was used to probe the impact of milling on the molecular structure together with computational studies. Figures 9 and 10 show the FTIR spectra of the crystalline nonmilled DABOMD, the amorphous standard, and the milled samples. The vibrational frequencies of some important functional groups of the crystalline nonmilled DABOMD are shown in Table 2.

As the milling progresses, broadening and disappearance of the FTIR peaks are evident for the milled samples (relative to the spectra of crystalline samples). Samples milled for 300 min exhibit very similar FTIR spectra to that of the reference amorphous DABOMD. Consistent with the results obtained

https://dx.doi.org/10.1021/acs.cgd.0c00770
Cryst. Growth Des. 2020, 20, 6057−6068

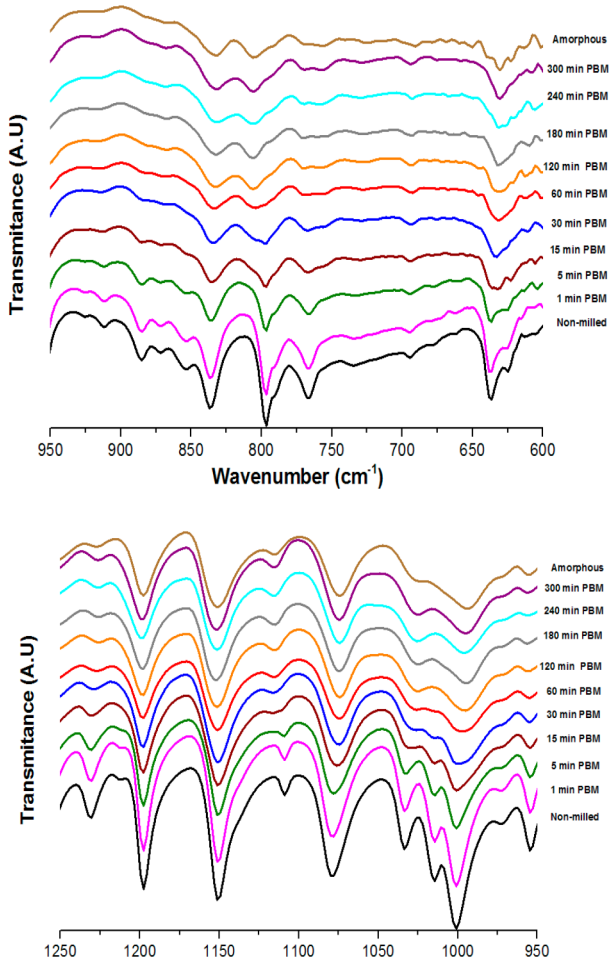

Figure 9. FTIR-ATR of nonmilled and milled DABOMD showing scans from (top) 600 to 950 cm^{-1}, (bottom) from 950 to 1250 cm^{-1}.

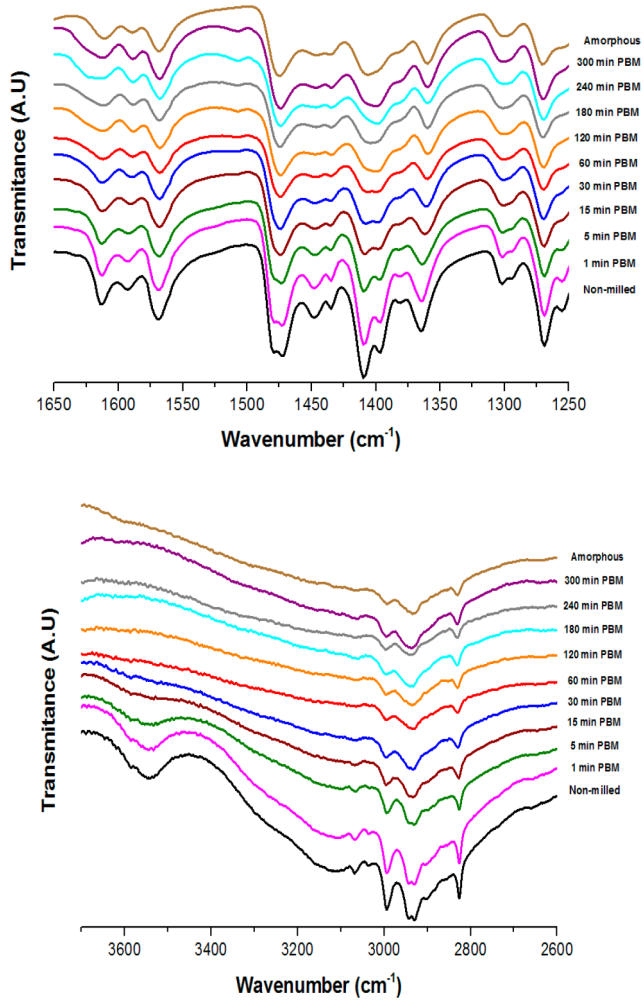

Figure 10. FTIR-ATR of nonmilled and milled DABOMD showing scans from (top) 1200 to 1600 cm^{-1} and (bottom) from 2600 to 3700 cm^{-1}

from PXRD, TGA, and DSC, the FTIR spectra thus confirm the formation of the amorphous form by milling. Marked changes in the spectral region's diagnostics for hydrogen bonding are also evident. The crystal structure (Figure 1a,b) shows that the two different waters (W1 and W2) are hydrogen bond donating to the pyridyl nitrogen (W2) and benzimidazole nitrogen (W1) of the DABOMD,[31] and in addition W1 and W2 form internal hydrogen bonds. The peaks for the crystalline nonmilled DABOMD are rather broad and not straightforward to individually assign. To try to assist in this, we performed density functional theory (DFT) calculations on a molecular system mimicking the crystal structure (see Figure S3 in the Supporting Information). From there, we observe that the vibrations involving the two waters are strongly coupled making the assignment of the experimental spectra with broad peaks challenging. However, we can clearly assign peaks in the region 3300−3600 cm^{-1} to O−H stretch modes, involving both W1 and W2. In addition, we tentatively assign the O−H stretch of W1 involving the hydrogen bonding to the benzimidazole nitrogen to the broad peak at 3130 cm^{-1}, but a more specific assignment of other peaks was not possible. However, the breaking of the hydrogen bonding pattern upon an elongated milling time is evident from the marked changes in the FTIR spectral regions corresponding to these O−H bands, in line with earlier studies.[33] The sharper peaks observed in the region 2800 to 3100 cm^{-1} we assign to mainly C−H stretches of the methyl and methoxy groups on the aromatic systems. As shown below,

Table 2. Mode of Vibration for the Main Functional Groups in DABOMD

functional group	type of vibration mode	crystalline vibration (cm^{-1})	amorphous vibration (cm^{-1})	300 min milled vibration (cm^{-1})
O−H	stretch	3300−3600	3070−3660	3070−3660
S═O	stretch	1001.2	993.9	994.9
C−H in CH_3 or O−CH_3	stretch	2929.5	2934.1	2935.7
benzimidazole H_3C−O	bend	1197.7	1197.8	1198.1

these groups are likely located at crystal cleavage planes and hence are affected by the milling as shown by the peak broadening. These FTIR results suggest that hydrogen bond breaking is associated with the amorphization of DABOMD in line with the TGA and DSC results of suggested hydrate water loss taking place.

3.2. Mechanism of Amorphization. The combined PXRD, DSC, TGA, and FTIR results revealed that DABOMD amorphization during milling can be attributed to the progressive release of water molecules. The distortion/breakage of their hydrogen bonds eventually leads to the collapse of the crystal lattice of DABOMD. There is a near absence of literature

https://dx.doi.org/10.1021/acs.cgd.0c00770
Cryst. Growth Des. 2020, 20, 6057−6068

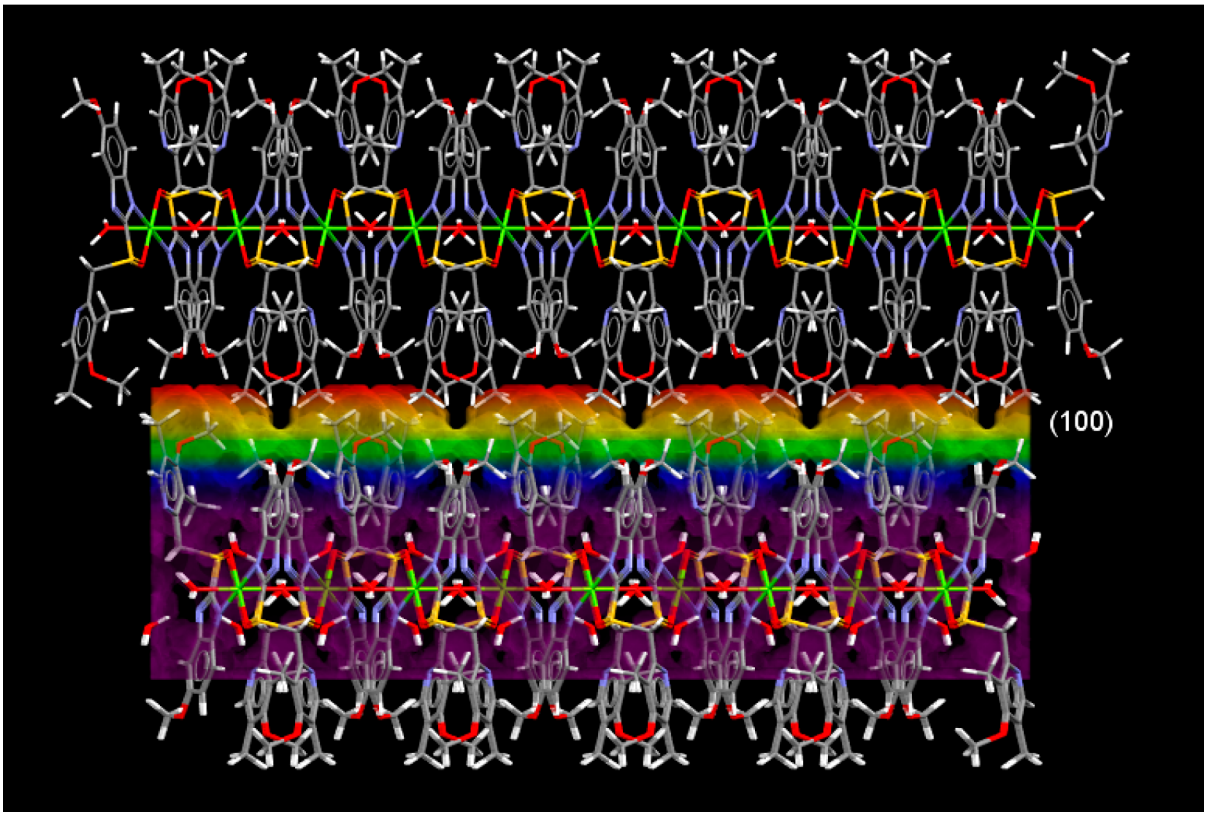

Figure 11. Visualization of the potential (100) slip plane in DABOMD crystal.

on studies probing the underlying mechanisms for amorphization during milling of organic crystals. Understanding the mechanically induced amorphization process requires a (i) thorough knowledge of the milling conditions and (ii) the underlying material properties of the feed, including its crystal structure and mechanical properties.

(i) In a planetary ball mill, the energy supplied to the particles gives rise to different forms of stress distribution including compression stress by impact and rolling, and shearing stress caused by sliding.[37]

(ii) The crystal structure of DABOMD involves hydrogen bonds of different strengths, which hold the crystal lattice. These stems from two loosely bonded water molecules and two strongly bounded water molecules as discussed earlier (Figure 1). Therefore, it can be suggested that the impact and the shearing from the mill can cause distortion/breakage of the hydrogen bonds and the release of water molecules simultaneously, as was indicated previously from the thermochemical and intermolecular analyses. This can make the crystals shear unstable and lead to the emergence of amorphous DABOMD. Also, the kinetic energy and the heat generated from the mill can increase the vibration of the water molecules promoting dehydration, dislocation, and accumulation of defects, hence speeding up the phase transformation of DABOMD.

Moreover, as evaluated in our previous study,[31] DABOMD exhibits a crystal slip plane, the (100) plane with weak hydrogen bonding across the plane (Figure 11). Other candidate slip planes can be (011), (11$\bar{1}$), and (102) given that they hold secondary morphological importance as shown in Table 3. Slip planes are the planes incorporating the weakest interactions

Table 3. DABOMD Important Morphological Planes Based on the Attachment Energy (E_{att}) Calculations[a]

(h k l)	multiplicity	d_{hkl} (Å)	total E_{att} (kcal mol^{-1})	area (%)
(1 0 0)	2	16.43	−25.8	59.4
(0 1 1)	4	6.89	−75.9	21.5
(1 1 $\bar{1}$)	4	6.80	−78.8	9.0
(1 1 0)	4	7.23	−80.9	2.0
(1 0 $\bar{2}$)	2	7.08	−101.7	8.1

[a]Reproduced with the permission of the International Union of Crystallography (IUCr).[31]

between neighboring planes in the crystalline lattice. When the crystal is subjected to stress, one would anticipate that the deformation will usually occur through slip of the crystal planes that are the easiest to displace, which promotes particle fracture.[38] Also, the dislocations and defects promote plastic deformation, which will ultimately lead to amorphization.[13] Analysis of the change in PXRD peaks upon milling shows that the most significant intensity change occurs for the peak at 2θ = 5.4 as illustrated in Figure 12 and (Table S1 in Supporting Information). This peak coincides with the major slip plane (100) to be mostly affected, while the effect of other planes is less straightforward to interpret. However, effects on the above-mentioned (011), (11$\bar{1}$), and (102) planes are also observed. In addition to the PXRD, the effect of crystal cleavage at plane (100) is reflected in the FTIR peak changes at 2800−3100 cm^{-1}, which represents the methoxy and methyl group respectively, which are designated around (100) (Figure 11). Therefore, we postulate that the shear and impact from milling causes the crystal to be cleaved along the easiest slip planes, and at a later stage also affect the hydrogen bond breakage, which leads to further crystalline disorder and amorphization. Therefore, it can

https://dx.doi.org/10.1021/acs.cgd.0c00770
Cryst. Growth Des. 2020, 20, 6057−6068

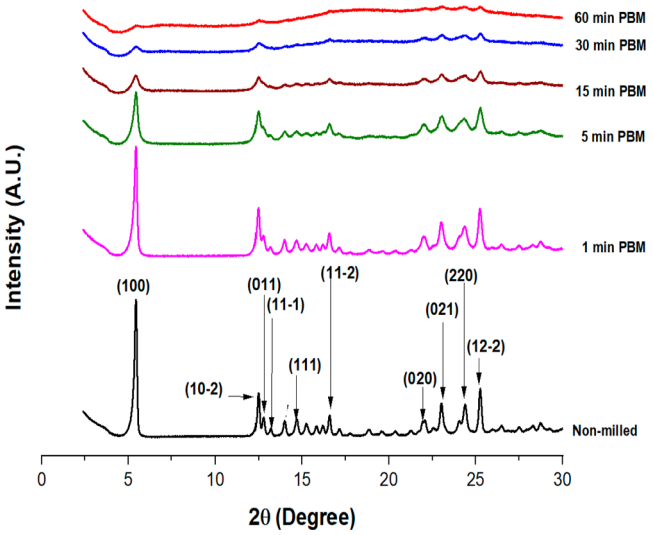

Figure 12. Identification of planes involved in the crystalline disorder of DABOMD.

be observed that milling has not only led to physical change of DABOMD but also caused a change reflected in the dehydration process. Another example of where mechanical activation leads to a form change is ampicillin trihydrate, which transforms into the amorphous form upon grinding. Takahashi et al. (1984) suggested that the freed water molecules from dehydration caused by grinding leads to the collapse of the crystal lattice.[39]

Various researchers have suggested amorphization as a result of vitrification (melt quench) at the surface.[40] Thermal PXRD was employed to evaluate the effect of the temperature increase (from 25 to 170 °C) on the mechanochemistry of DABOMD. It appears from Figure 13 that the crystallinity starts to effectively

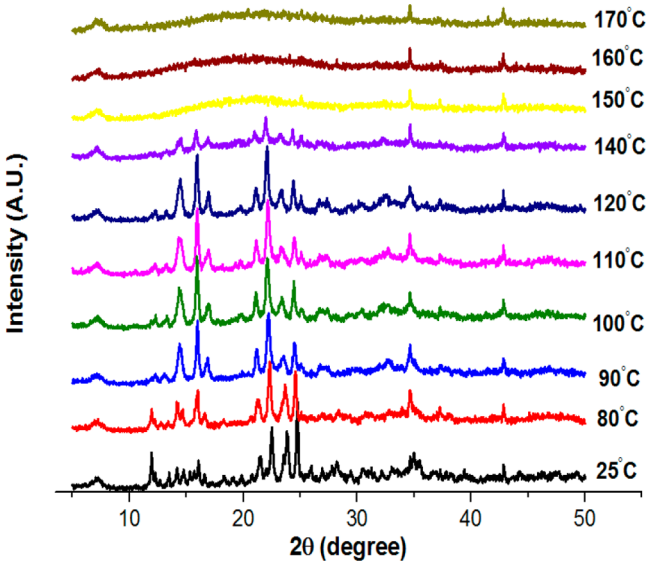

Figure 13. Thermal controlled PXRD of DABOMD from 25 to 170 °C.

vanish above 120 °C, which suggests that high temperature can be a contributing factor to the amorphization of DABOMD. The temperature contribution is composed of the bulk temperature and the localized temperature. The bulk temperature is the temperature of the mill, which was measured by the authors of ref 41 who found that the highest temperature obtained was 80 °C. The localized temperature is the temperature generated on the submicron regions on the impacting surfaces, which can be much higher than the bulk temperature, but it is very difficult to measure.[8]

In summary, the amorphization of DABOMD is therefore associated with the following events: crystal cleavage via slip of planes, water loss, accumulation of defects, and distortion of the hydrogen bonds holding the crystal backbone as a result of stresses and temperature experienced during the milling process. The order of these events has been further investigated with a study of the kinetics. Slip of planes can promote particle fracture and creation of new surfaces. The release of water molecules can create dislocation sites that facilitate the slip, accumulation of defects, and plastic deformation. Increased temperatures can lead to dehydration, increased atomic mobility, and hence distortion of the crystalline lattice and may also lead to surface melt and formation of amorphous upon cooling.

3.3. Kinetics of Comminution and Amorphization. Prolonged milling of DABOMD resulted in significant (i) comminution represented by a change in D_{90} (Table 1) and (ii) large amorphization indicated by amorphous content (AAC) detected by FTIR chemometric analysis (Table 4) and 50%

Table 4. Percentage Amorphous Quantified Using the FTIR Chemometric Method of Milled DABOMD and Equivalent % Water Content from TGA

	amorphous content		% water content
milling time (min)	first derivative	second derivative	TGA
0	0	0	8.7
1	0.101	0.12	8.3
5	0.356	0.223	7.7
15	0.713	0.632	7.2
30	0.828	0.712	6.5
60	0.908	0.708	5.9
120	0.933	0.822	5.3
180	0.999	0.977	4.7
240	0.999	0.943	4.3
300	1	0.961	4.2

water loss (WL), indicated from TGA quantification (Table 4). The changes in comminution, amorphization, and the amount of water follow an exponential pattern as shown in (experimental) Figure 14, panels a, b, and c, respectively. Looking at Figure 14a (experimental), it appears that the process of comminution depicts two sequential processes: a rapid comminution (first 15 min), and a slow comminution. Similarly, Figure 14b (experimental) representing the amorphization process shows two sequential processes; a rapid amorphization and a slow amorphization process. Interestingly the water loss process (Figure 14c) also seems to occur in two sequential events; a rapid water loss and a slow water loss event. This further enhances the interpretation that loss of water is associated with the change of DABOMD.

In order to facilitate a quantitative description of the comminution, amorphization, and water loss events, we represent the mechanisms with parallel first order processes characterized by a time constant. This is first applied to the D_{90}; we define the extent of comminution, x_{com}, as the fraction of change in D_{90} compared to the total change in its value. The extent that comminution reduces from 1 to zero in an exponential fashion that could be modeled as a two parallel

https://dx.doi.org/10.1021/acs.cgd.0c00770
Cryst. Growth Des. 2020, 20, 6057−6068

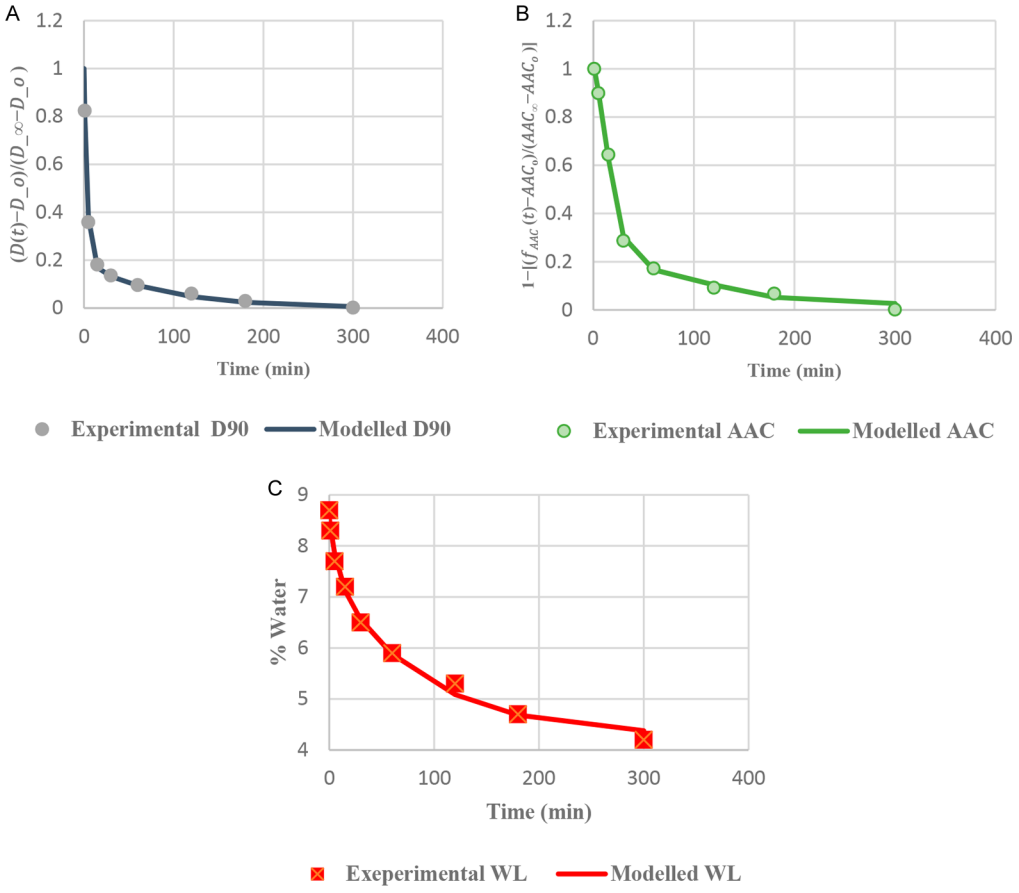

Figure 14. Experimental and modeled comminution and amorphization of DABOMD with respect to time.

rate process because their time constants vary by an order of magnitude:

$$x_{com} = \frac{D(t) - D_o}{D_\infty - D_o} = \alpha_{rpd\_com} e^{-t/\tau_{rpd\_com}} + (1 - \alpha_{rpd\_com}) e^{-t/\tau_{slw\_com}} \quad (5)$$

Here, $D(t)$ is the D_{90} of the milled sample at time t, and D_o, D_∞, the D_{90} at the start and end of the milling process, respectively. The time constants τ_{rpd_com}, τ_{frac} are the time scales for rapid comminution. Figure 14b (modeled) two parallel processes for the loss of crystallinity (amorphization), characterized here by the extent of crystallinity, x_{cryst} which is obtained from the apparent amorphous content, $f_{AAC}(t)$ as determined from the chemometric analysis of the FTIR data as outlined in section 2.2.2.

$$x_{cryst} = 1 - \frac{f_{AAC}(t) - AAC_o}{AAC_\infty - AAC_o} = \alpha_{rpd\_amp} e^{-t/\tau_{rpd\_amp}} + (1 - \alpha_{rpd\_amp}) e^{-t/\tau_{slw\_com}} \quad (6)$$

Here, AAC_o, $f_{AAC}(t)$, and AAC_∞ are the apparent amorphous content of the milled sample at time $t = 0$, t and at the end of the milling period respectively.

For completeness, the parameters α_{rpd_com}, α_{rpd_amp} and time constants τ_{rpd_com}, τ_{slw_com}, and τ_{rpd_amp} in eqs 5 and 6 were quantified by minimizing the sum of squares between the measured and predicted extend of comminution and crystallinity according to eq 7:

$$SOS = \sum_{i=1}^{9} [x_{com.meas}(t_i) - x_{com.calc}(t_i)]^2 + \sum_{i=1}^{9} [x_{cryst.meas}(t_i) - x_{cryst.calc}(t_i))]^2 \quad (7)$$

The water loss event can be modeled by fitting it to the rate constants representing the extent of comminution as shown in eq 8.

$$\%water = 4.27(1 + 0.74e^{-t/\tau_{rpd\_amp}} + 0.26e^{-t/\tau_{slw\_com}}) \quad (8)$$

The outcome of fitting the data shows the following:

The model fitted to the comminution data (Figure 14 a, modeled) results in α_{rpd_com} = 81%, τ_{rpd_com} = 3.6 min, and τ_{slw_com} = 88.3 min; this confirms that rapid comminution accounts for 80% of the extent of comminution. The slower comminution occurs at a much slower time scale (88.3 min), which indicates that if comminution is considered complete when x_{com} < 1%, then, the comminution is complete after approximately 300 min ($x_{com} = 0.2e^{-300/88}$). It is worth noting that the time scale τ represents the inverse of the rate constant k. The time scale allows us to see the sequence of events.

The model fitted to the amorphization data (Figure 14b, modeled) resulting in α_{rpd_amp} = 79% and τ_{rpd_amp} = 8 min. The final time constant is identical to the time scale of rapid comminution in eq 5 which emphasizes that about 80% of amorphization occurs in the first few minutes of milling.

The model fitted to the water content data (Figure 14c, modeled) shows that at τ_{rpd_amp} = 8 min, the % water = 1.106,

https://dx.doi.org/10.1021/acs.cgd.0c00770
Cryst. Growth Des. 2020, 20, 6057−6068

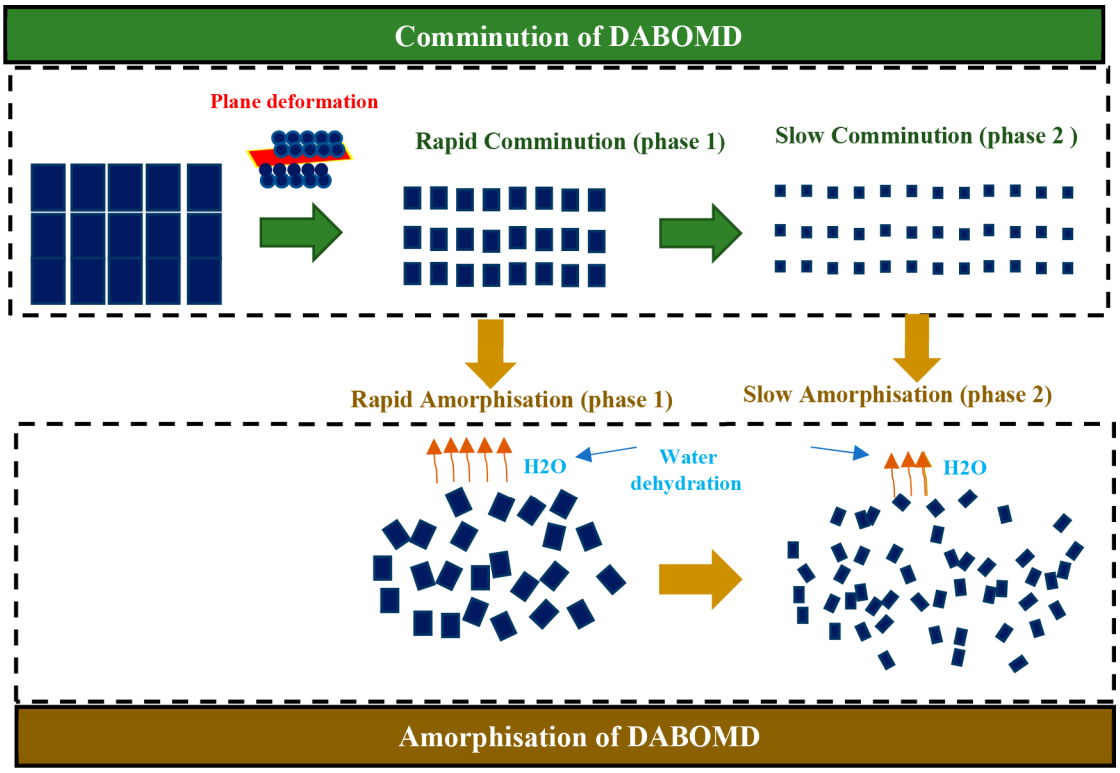

Figure 15. Proposed mechanistic model for the milling process of DABOMD; ordered blue particles represent the comminution process and disordered blue particles represent amorphization.

which is equivalent to 15% water loss during the first event (in the first 15 min of milling as was indicated by TGA). This further enhances that water loss is clearly associated with the rapid amorphization since they both occur at the same time scale of ca. 8 min.

We can finally propose a comprehensive mechanism that shows the sequential events occurring during the milling of DABOMD following Figure 15. (1) We believe that the first process that occurs at the time scale of 4 min is the crystal cleavage via slip of planes, which accounts for the rapid comminution (size reduction + deagglomeration) which creates a large number of fresh surfaces and defects. (2) The created surfaces allow for fast diffusion reflected in the rapid evaporation of water molecules from the crystalline lattice. The deformation of planes, dislocation, and mobility of the water molecules cause breakage and disruption of the hydrogen bonds in the lattice accounting for the rapid amorphization observed in the time scale of 8 min. (3) The slower event of comminution is attributed to decrease of the number of slip planes and the amount of generated defect. This implies that fewer surfaces are available for water diffusion, which explains the drop of water dehydration and hence slower amorphization.

4. CONCLUSION

The study of mechanochemistry is very limited in pharmaceuticals materials. This paper describes a combined experimental and modeling approach to investigate the mechanochemistry of DABOMD. The experimental work involved milling DABOMD at different times in a planetary ball mill and carrying out a full characterization of the feed and the product morphological, crystalline, thermodynamic, and intermolecular properties. Milling of DABOMD causes a prominent comminution within 60 min of milling. A mathematical model fit of comminution and the amorphization were performed to evaluate the kinetic aspects that DABOMD undergoes upon milling. The outcome of the fit shows that initially, 80% of the particle's comminution occurs by crystal cleavage via the slip of planes occurring in a time scale of 4 min. This is followed by a rapid dehydration (of approximately 20% of the water content), which occurs within a time scale of 8 min. The planes deformation along with rapid dehydration of water results in loss of 80% of the crystallinity, with the remaining 20% lost during subsequent comminution in a time scale of 100 min, resulting from limited slip planes and surfaces available for water diffusion. The method applied connects the intrinsic characteristics of the particles at the molecular level (i.e., crystalline structure, mechanical properties) and the bulk properties that can be influenced by process parameters (type of stress, energy, time). The implementation of this methodology requires an in-depth understanding of the underlying intrinsic material properties at the molecular level, which was performed in previous work and knowledge of the milling environment and parameters. This approach can be successfully applied in the study of any change arising with milling, i.e., comminution and or/mechanochemistry, and can also be implemented in other pharmaceutical processes.

■ ASSOCIATED CONTENT

Supporting Information

The Supporting Information is available free of charge at https://pubs.acs.org/doi/10.1021/acs.cgd.0c00770.

Additional SEMs, Miller plans, and DABOMD structure used for calculation of molecular IR spectra (PDF)

https://dx.doi.org/10.1021/acs.cgd.0c00770
Cryst. Growth Des. 2020, 20, 6057−6068

AUTHOR INFORMATION

Corresponding Authors

Michael J. Quayle − *New Modalities and Parenteral Development, Pharmaceutical Technology & Development, Operations, AstraZeneca, Gothenburg, Sweden;* orcid.org/0000-0001-5782-6506; Email: mike.quayle@astrazeneca.com

Ali Hassanpour − *School of Chemical and Process Engineering, University of Leeds, Leeds LS2 9JT, U.K.;* orcid.org/0000-0002-7756-1506; Email: a.hassanpour@leeds.ac.uk

Authors

Hanane Abouhakim − *School of Chemical and Process Engineering, University of Leeds, Leeds LS2 9JT, U.K.;* orcid.org/0000-0003-2581-8442

Stefan T. Norberg − *Oral Product Development, Pharmaceutical Technology & Development, Operations, AstraZeneca, Gothenburg, Sweden;* orcid.org/0000-0003-4556-1920

Sten O. Nilsson Lill − *Early Product Development and Manufacturing, Pharmaceutical Sciences, R&D, AstraZeneca, SE-431 83 Mölndal, Sweden;* orcid.org/0000-0003-4818-8084

Maryam Asachi − *School of Chemical and Process Engineering, University of Leeds, Leeds LS2 9JT, U.K.;* orcid.org/0000-0002-9112-4839

Sven L. M. Schroeder − *School of Chemical and Process Engineering, University of Leeds, Leeds LS2 9JT, U.K.;* orcid.org/0000-0002-4232-5378

Frans L. Muller − *School of Chemical and Process Engineering, University of Leeds, Leeds LS2 9JT, U.K.;* orcid.org/0000-0002-8507-4193

Complete contact information is available at: https://pubs.acs.org/10.1021/acs.cgd.0c00770

Funding

The following funding is acknowledged: Engineering and Physical Sciences Research Council; AstraZeneca and University of Leeds.

Notes

The authors declare no competing financial interest.

REFERENCES

(1) Todres, Z. V. *Organic Mechanochemistry and Its Practical Applications*; CRC/Taylor & Francis, 2006.

(2) Khadka, P.; Ro, J.; Kim, H.; Kim, I.; Kim, J. T.; Kim, H.; Cho, J. M.; Yun, G.; Lee, J. Pharmaceutical Particle Technologies: An Approach to Improve Drug Solubility, Dissolution and Bioavailability. *Asian J. Pharm. Sci.* **2014**, *9*, 304−316.

(3) Trasi, N. S.; Byrn, S. R. Mechanically Induced Amorphization of Drugs: A Study of the Thermal Behavior of Cryomilled Compounds. *AAPS PharmSciTech* **2012**, *13*, 772−784.

(4) Shah, B.; Kakumanu, V. K.; Bansal, A. K. Analytical Techniques for Quantification of Amorphous/Crystalline Phases in Pharmaceutical Solids. *J. Pharm. Sci.* **2006**, *95*, 1641−1665.

(5) Haleblian, J.; Mccrone, W. Pharmaceutical Applications of Polymorphism. *J. Pharm. Sci.* **1969**, *58*, 911−929.

(6) Snow, R. H.; Luckie, P. T. Annual Review of Size Reduction. *Powder Technol.* **1979**, *23*, 31−46.

(7) Chieng, N.; Aaltonen, J.; Saville, D.; Rades, T. Physical Characterization and Stability of Amorphous Indomethacin and Ranitidine Hydrochloride Binary Systems Prepared by Mechanical Activation. *Eur. J. Pharm. Biopharm.* **2009**, *71*, 47−54.

(8) Colombo, I.; Grassi, G.; Grassi, M. Drug Mechanochemical Activation. *J. Pharm. Sci.* **2009**, *98*, 3961−3986.

(9) Descamps, M.; Willart, J. F. Perspectives on the Amorphisation/Milling Relationship in Pharmaceutical Materials. *Adv. Drug Delivery Rev.* **2016**, *100*, 51−66.

(10) Takacs, L. The Historical Development of Mechanochemistry. *Chem. Soc. Rev.* **2013**, *42*, 7649.

(11) Brittain, H. G. *Profiles of Drug Substances, Excipients and Related Methodology*; Elsevier, 2010.

(12) Caron, V.; Tajber, L.; Corrigan, O. I.; Healy, A. M. A Comparison of Spray Drying and Milling in the Production of Amorphous Dispersions of Sulfathiazole/Polyvinylpyrrolidone and Sulfadimidine/Polyvinylpyrrolidone. *Mol. Pharmaceutics* **2011**, *8*, 532−542.

(13) Balaz, P.; Achimovicova, M.; Balaz, M.; Billik, P.; Cherkezova-Zheleva, Z.; Criado, J. M.; Delogu, F.; Dutkova, E.; Gaffet, E.; Gotor, F. J.; Kumar, R.; Mitov, I.; Rojac, T.; Senna, M.; Streletskii, A.; Wieczorek-Ciurowa, K. Hallmarks of Mechanochemistry: From Nanoparticles to Technology. *Chem. Soc. Rev.* **2013**, *42*, 7571−7637.

(14) Boldyrev, V. V. Mechanochemical Modification and Synthesis of Drugs. *J. Mater. Sci.* **2004**, *39*, 5117−5120.

(15) Otsuka, M.; Otsuka, K.; Kaneniwa, N. Relation Between Polymorphic Transformation Pathway During Grinding and the Physicochemical Properties of Bulk Powders for Pharmaceutical Preparations. *Drug Dev. Ind. Pharm.* **1994**, *20*, 1649−1660.

(16) Shakhtshneider, T. P. Phase Transformations and Stabilization of Metastable States of Molecular Crystals under Mechanical Activation. *Solid State Ionics* **1997**, *101*, 851−856.

(17) Mahlin, D.; Bergström, C. A. S. Early Drug Development Predictions of Glass-Forming Ability and Physical Stability of Drugs. *Eur. J. Pharm. Sci.* **2013**, *49*, 323−332.

(18) Renata Toplak Casar, L. (SI). Process for the Preparation of Esomeprazole Magnesium Dihydrate. US 8,362.259 B2, 2013.

(19) Agatonovic-Kustrin, S.; Markovic, N.; Ginic-Markovic, M.; Mangan, M.; Glass, B. D. Compatibility Studies between Mannitol and Omeprazole Sodium Isomers. *J. Pharm. Biomed. Anal.* **2008**, *48*, 356−360.

(20) Willart, J.-F.; Durand, M.; Briggner, L.-E.; Marx, A.; Danede, F.; Descamps, M. Solid-State Amorphization of Linaprazan by Mechanical Milling and Evidence of Polymorphism. *J. Pharm. Sci.* **2013**, *102*, 2214−2220.

(21) Descamps, M.; Willart, J. F.; Dudognon, E.; Caron, V. Transformation of Pharmaceutical Compounds upon Milling and Comilling: The Role of Tg. *J. Pharm. Sci.* **2007**, *96*, 1398−1407.

(22) Shakhtshneider, T. P.; Boldyrev, V. V. Phase Transformations in Sulfathiazole During Mechanical Activation. *Drug Dev. Ind. Pharm.* **1993**, *19*, 2055−2067.

(23) Mesallati, H.; Conroy, D.; Hudson, S.; Tajber, L. Preparation and Characterization of Amorphous Ciprofloxacin-Amino Acid Salts. *Eur. J. Pharm. Biopharm.* **2017**, *121*, 73−79.

(24) De Gusseme, A.; Neves, C.; Willart, J. F.; Rameau, A.; Descamps, M. Ordering and Disordering of Molecular Solids upon Mechanical Milling: The Case of Fananserine. *J. Pharm. Sci.* **2008**, *97*, 5000−5012.

(25) Chauruka, S. R.; Hassanpour, A.; Brydson, R.; Roberts, K. J.; Ghadiri, M.; Stitt, H. Effect of Mill Type on the Size Reduction and Phase Transformation of Gamma Alumina. *Chem. Eng. Sci.* **2015**, *134*, 774−783.

(26) Bochevarov, A. D.; Harder, E.; Hughes, T. F.; Greenwood, J. R.; Braden, D. A.; Philipp, D. M.; Rinaldo, D.; Halls, M. D.; Zhang, J.; Friesner, R. A. Jaguar: A High-Performance Quantum Chemistry Software Program with Strengths in Life and Materials Sciences. *Int. J. Quantum Chem.* **2013**, *113*, 2110−2142.

(27) Nilsson Lill, S. O.; Siegbahn, E. M. *Biochemistry* **2009**, *48*, 1056−1066, DOI: 10.1021/bi801218n.

(28) Asachi, M.; Hassanpour, A.; Ghadiri, M.; Bayly, A. Assessment of Near-Infrared (NIR) Spectroscopy for Segregation Measurement of Low Content Level Ingredients. *Powder Technol.* **2017**, *320*, 143−154.

(29) Vanarase, A. U.; Järvinen, M.; Paaso, J.; Muzzio, F. J. *Powder Technology* **2013**, *241*, 263−271, DOI: 10.1016/j.powtec.2013.02.012.

(30) Johanson, K. Review of New Segregation Tester Method by Dr. Kerry Johanson, P.E. *Powder Technol.* **2014**, *257*, 1−10.

(31) Abouhakim, H.; Nilsson Lill, S. O.; Quayle, M. J.; Norberg, S. T.; Hassanpour, A.; Pask, C. M. The Crystal Structure, Morphology and Mechanical Properties of Diaquabis(Omeprazolate)Magnesium Dihydrate. *Acta Crystallogr., Sect. B: Struct. Sci., Cryst. Eng. Mater.* **2020**, *76*, 275−284.
(32) Reddy, M. S.; Pradesh, A.; Kumar, M. K.; Purandhar, K.; Sreenath, K. Amorphous hydrates of esomeprazole magnesiumand process for the preparation thereof. US 2004/0167173 A1, 2004.
(33) Murakami, F. S.; Lang, K. L.; Mendes, C.; Cruz, A. P.; Filho, M. A. S. C.; Silva, M. A. S. Physico-Chemical Solid-State Characterization of Omeprazole Sodium: Thermal, Spectroscopic and Crystallinity Studies. *J. Pharm. Biomed. Anal.* **2009**, *49*, 72−80.
(34) Kaushal, A. M.; Chakraborti, A. K.; Bansal, A. K. FTIR Studies on Differential Intermolecular Association in Crystalline and Amorphous States of Structurally Related Non-Steroidal Anti-Inflammatory Drugs. *Mol. Pharmaceutics* **2008**, *5*, 937−945.
(35) Stephenson, G. A.; Forbes, R. A.; Reutzel-Edens, S. M. Characterization of the Solid State: Quantitative Issues. *Adv. Drug Delivery Rev.* **2001**, *48*, 67−90.
(36) Markovic, N.; Agotonovic-Kustrin, S.; Glass, B.; Prestidge, C. A. Physical and Thermal Characterisation of Chiral Omeprazole Sodium Salts. *J. Pharm. Biomed. Anal.* **2006**, *42*, 25−31.
(37) Young, P. M.; Chan, H.-K.; Chiou, H.; Edge, S.; Tee, T. H. S.; Traini, D. The Influence of Mechanical Processing of Dry Powder Inhaler Carriers on Drug Aerosolization Performance. *J. Pharm. Sci.* **2007**, *96*, 1331−1341.
(38) Halme, A.; Quayle, M. J.; Nilsson Lill, S. O.; Pettersen, A.; Fransson, M.; Boissier, C. Utilizing Crystal Structures for Predicting Impact of Mechanical and Surface Properties on Particle Fracture. *Cryst. Growth Des.* **2019**, *19*, 3670−3680.
(39) Takahashi, Y.; Nakashima, K.; Nakagawa, H.; Sugimoto, I. Effects of Grinding and Drying on the Solid-State Stability of Ampicillin Trihydrate. *Chem. Pharm. Bull.* **1984**, *32*, 4963−4970.
(40) Descamps, M.; Aumelas, A.; Desprez, S.; Willart, J. F. The Amorphous State of Pharmaceuticals Obtained or Transformed by Milling: Sub-Tg Features and Rejuvenation. *J. Non-Cryst. Solids* **2015**, *407*, 72−80.
(41) Chauruka, S. R. *Effect of Milling on Size Reduction and Microstructural Changes to Gamma-Alumina*; The University of Leeds, 2015.

https://dx.doi.org/10.1021/acs.cgd.0c00770
Cryst. Growth Des. 2020, 20, 6057−6068